8

Magnetic Stirring Using Rotating Fields

Liquid metals freeze in much the same way as water. First, snowflake-like crystals form, and as these multiply and grow a solid emerges. However, this solid can be far from homogeneous. Just as a chef preparing ice-cream has to beat and stir the partially solidified cream to break up the crystals and release any trapped gas, so many steelmakers have to stir partially solidified ingots to ensure a fine-grained, homogeneous product. The preferred method of stirring is electromagnetic, and has been dubbed the 'electromagnetic teaspoon'. We shall describe this process shortly. First, however, it is necessary to say a little about commercial casting processes.

8.1 Casting, Stirring and Metallurgy

> It will emerge from dark and gloomy caverns, casting all human races into great anxiety, peril and death. It will take away the lives of many; with this men will torment each other with many artifices, traductions and treasons. O monstrous creature, how much better it would be if you were to return to hell
>
> *(Leonardo da Vinci on the extraction and casting of metals)*

Man has been casting metals for quite some time. Iron blades, perhaps 5000 years old, have been found in Egyptian pyramids, and by 1000 BC we find Homer mentioning the working and hardening of steel blades. Until relatively recently, all metal was cast by a batch process involving pouring the melt into closed moulds. However, today the bulk of aluminium and steel is cast in a continuous fashion, as indicated in Figure 8.1. In brief, a solid ingot is slowly withdrawn from a liquid-metal pool, the pool being continuously replenished from above. In the case of steel, which has a low thermal diffusivity, the pool is long and deep, resembling a long liquid-metal column. For aluminium, however, the pool is roughly hemispherical in shape, perhaps 0.5 m in diameter. Casting speeds are of the order of a few mm/s.

Downloaded from https://www.cambridge.org/core. NYU School of Medicine, on 13 Nov 2018 at 19:51:53, subject to the Cambridge Core terms of use, available at https://www.cambridge.org/core/terms. https://doi.org/10.1017/CBO9780511623332.011
Cambridge Books Online © Cambridge University Press, 2010

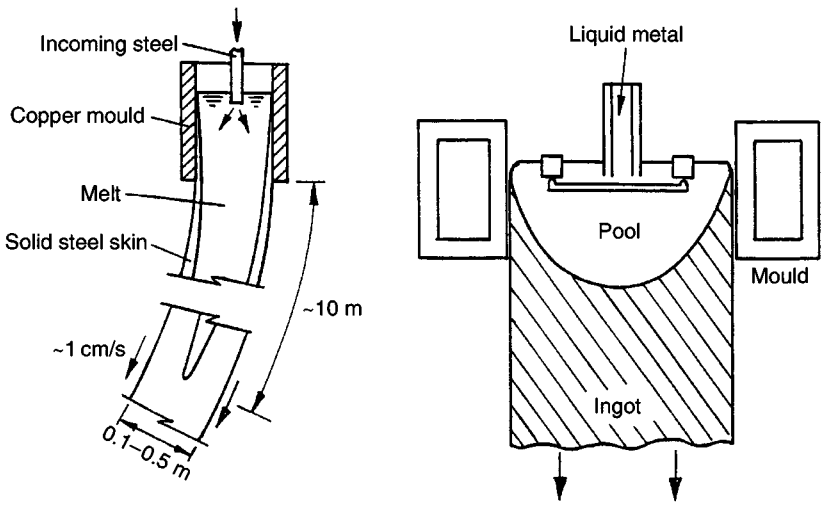

Figure 8.1 (a) Casting of steel; (b) casting of aluminium.

Unfortunately, ingots cast in this manner are far from homogeneous. For example, during solidification alloying elements tend to segregate out of the host material, giving rise to inhomogeneities in the final structure. This is referred to as *macro-segregation*[1]. Moreover, small cavities can form on the ingot surface or near the centre-line. Surface cavities are referred to as blow holes or pin holes, and arise from the formation of gas bubbles (CO or N_2 in the case of steel). Centre-line porosity, on the other hand, is associated with shrinkage of the metal during freezing.

All of these defects can be alleviated, to some degree, by stirring the liquid pool (Birat & Chone, 1983; Takeuchi et al., 1992). This is most readily achieved using a rotating magnetic field, as shown in Figure 8.2. The stirring has the added benefit of promoting the nucleation and growth of *equi-axed crystals* (crystals like snowflakes) at the expense of *dendritic crystals* (those like fir-trees) which are large, anisotropic and generally undesirable. In addition to these metallurgical benefits, it has been found that stirring has a number of incidental operational advantages, such as allowing higher casting temperatures and faster casting rates (Marr, 1984).

[1] Macro-segregation was a recognized problem in casting as far back as 1540, when Biringuccio described macro-segregation problems in the production of gun barrels.

Downloaded from https://www.cambridge.org/core. NYU School of Medicine, on 13 Nov 2018 at 19:51:53, subject to the Cambridge Core terms of use, available at https://www.cambridge.org/core/terms. https://doi.org/10.1017/CBO9780511622533.011
Cambridge Books Online © Cambridge University Press, 2010

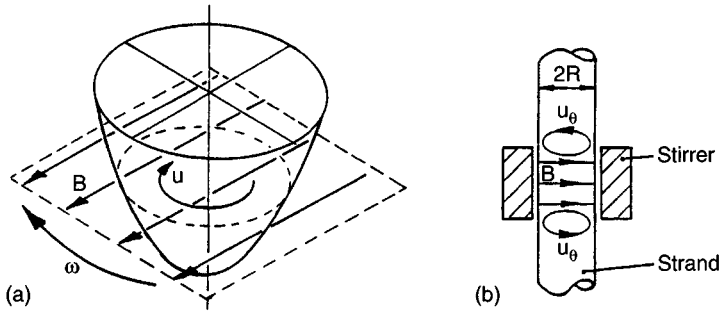

Figure 8.2 (a) Magnetic stirring of aluminium; (b) stirring of steel.

The perceived advantages of magnetic stirring led to a widespread implementation of this technology in the 1980s, particularly in the steel industry. In fact, by 1985, some 20% of slab casters (casters producing large steel ingots) and 50% of bloom casters (casters producing medium-sized steel ingots) had incorporated magnetic stirring.

However, this was not the end of the story. While some manufacturers reported significant benefits, others encountered problems. For example, in steel-making excessive stirring can lead to the entrainment of debris from the free surface and to a thinning of the solid steel shell at the base of the mould. This latter phenomenon is particularly dangerous as it can lead to a rupturing of the solid skin. Different problems were encountered in the aluminium industry. Here it was found that, in certain alloys, macrosegregation was aggravated (rather than reduced) by stirring, possibly because centrifugal forces tend to separate out crystal fragments of different composition.

By the mid-1980s it was clear that there was a need to rationalise the effects of magnetic stirring and this, in turn, required that metallurgists and equipment manufacturers develop a quantitative picture of the induced velocity field. The first, simple models began to appear in the early 1980s, usually based on computer simulations. However, these were somewhat naive and the results rather misleading. The difficulty arose because early researchers (quite naturally) tried to simplify the problem, and an obvious starting point was to consider a two-dimensional idealisation of the process. Unfortunately, it turns out that the key dynamical processes are all three-dimensional, and so two-dimensional idealisations of magnetic stirring are hopelessly inadequate. We shall describe both the early two-dimensional models and their more realistic three-dimensional counterparts in the subsequent sections.

Downloaded from https://www.cambridge.org/core. NYU School of Medicine, on 13 Nov 2018 at 19:51:53, subject to the Cambridge Core terms of use, available at https://www.cambridge.org/core/terms. https://doi.org/10.1017/CBO9780511623332.011
Cambridge Books Online © Cambridge University Press, 2010

There are many ways of inducing motion in a liquid-metal pool. The most common means of stirring is to use a rotating, horizontal magnetic field, an idea which dates back to 1932. The field acts rather like an induction motor, with the liquid taking the place of the rotor (Figure 8.3a). In practice, a rotating magnetic field may be generated in a variety of ways, each producing a slightly different spatial structure for **B**. (The

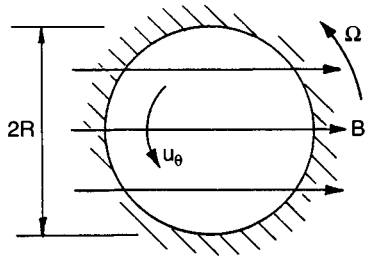

Figure 8.3 (a) A one-dimensional model of stirring.

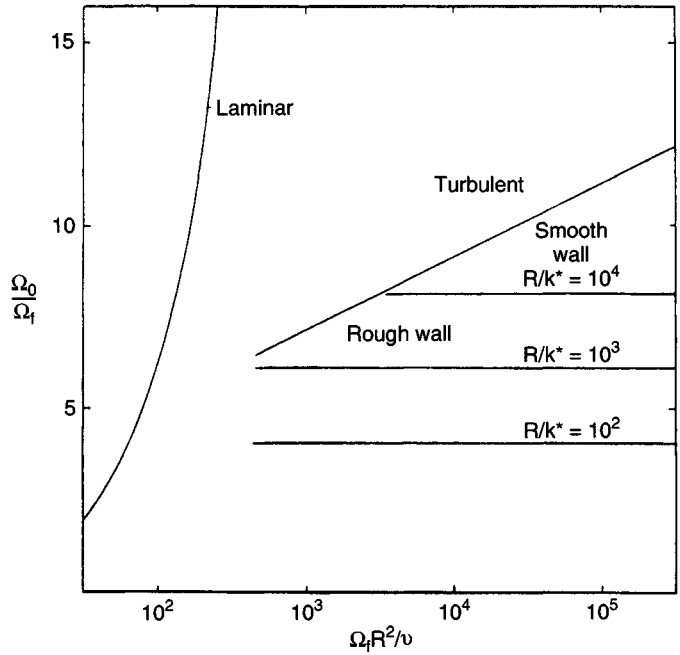

Figure 8.3 (b) Core angular velocity versus Ω_f for one-dimensional flow.

Downloaded from https://www.cambridge.org/core. NYU School of Medicine, on 13 Nov 2018 at 19:51:53, subject to the Cambridge Core terms of use, available at https://www.cambridge.org/core/terms. https://doi.org/10.1017/CBO9780511533313.011
Cambridge Books Online © Cambridge University Press, 2010

field is never perfectly uniform nor purely horizontal.) However, the details do not matter. The key point is that a rotating magnetic field, which is predominantly horizontal, induces a time-averaged Lorentz force which is a prescribed function of position, is independent of the velocity of the metal, and whose dominant component is azimuthal: $(0, F_\theta, 0)$ in (r, θ, z) coordinates. The important questions are: (i) How does the induced velocity scale with the Lorentz force? (ii) Does the induced swirl $(0, u_\theta, 0)$ have a spatial structure which mimics the spatial variations of the applied Lorentz force (i.e. strong swirl in regions where F_θ is intense and weak swirl where F_θ is low)? (iii) Are there significant secondary flows $(u_r, 0, u_z)$? To cut a long story short, the answers turn out to be:

(i) $u_\theta \sim B$
(ii) u_θ does *not* mimic the spatial variations in the Lorentz force;
(iii) the secondary flows are intense and dominate the dynamics of the liquid metal.

It is the subtle, yet critical, rôle played by the secondary flows which invalidates the results of the early, two-dimensional models and which makes this problem more interesting than it might otherwise be.

8.2 Early Models of Stirring

The first step in predicting the spatial structure of **u** is to determine the Lorentz force. Fortuitously, the magnitude and distribution of the time-averaged Lorentz force is readily calculated. There are two reasons for this. First, the magnetic field associated with the current induced in the liquid metal is almost always negligible by comparison with the imposed field, **B** (see, for example, Davidson & Hunt, 1987.) Faraday's law then gives the electric field as

$$\nabla \times \mathbf{E} = -\partial \mathbf{B}_0 / \partial t \tag{8.1}$$

where $\mathbf{B}_0$ is the known, imposed magnetic field. Second, the induced velocities are generally so low (by comparison with the rate of rotation of the **B**-field) that Ohm's law reduces to

$$\mathbf{J} = \sigma \mathbf{E} \tag{8.2}$$

Downloaded from https://www.cambridge.org/core. NYU School of Medicine, on 13 Nov 2018 at 19:51:53, subject to the Cambridge Core terms of use, available at https://www.cambridge.org/core/terms. https://doi.org/10.1017/CBO9780511623332.011
Cambridge Books Online © Cambridge University Press, 2010

Consequently, **E** (and hence **J**) may be found directly by uncurling (8.1) and the Lorentz force follows. In fact, we have already seen an example of just such a calculation in Chapter 5, Section 5.1. Here we evaluated the time-averaged Lorentz force generated by a uniform magnetic field rotating about an infinitely long, liquid-metal column. The force is

$$\mathbf{F} = \frac{1}{2}\sigma B^2 \Omega r \hat{\mathbf{e}}_\theta \tag{8.3}$$

where Ω is the field rotation rate and r is the radial coordinate. The restrictions on this expression are

$$u_\theta \ll \Omega R \leq \lambda/R, \qquad \lambda = (\mu\sigma)^{-1} \tag{8.4}$$

where R is the radius of the column. However, these conditions are almost always satisfied in practice. The first inequality, $u_\theta \ll \Omega R$, is precisely the condition required to ignore $\mathbf{u} \times \mathbf{B}$ in Ohm's law, while the second, $\Omega R \leq \lambda/R$, is equivalent to saying that R_m (based on ΩR) is small, so that the induced magnetic field is negligible.

Of course, for more complicated distributions of **B** we cannot use (8.3). Nevertheless, for almost any rotating field the Lorentz force is predominantly azimuthal, and on dimensional grounds it must be of order $\sigma B^2 \Omega R$ (provided that (8.4) is satisfied). Moreover, for fields which are symmetric about a plane through the origin, the Lorentz force must vanish on the axis. It follows that rotating, symmetric magnetic fields which satisfy (8.4) will induce a force of the form

$$\mathbf{F} = \left[\frac{1}{2}\sigma \Omega B_0^2 r\right] f(\mathbf{x}/R)\hat{\mathbf{e}}_\theta \tag{8.5}$$

Here B_0 is some characteristic field strength, and f is a function of order unity whose spatial distribution depends on that of **B** and whose exact form can be determined by uncurling (8.1). When **B** is uniform, $f = 1$.

We now consider the dynamical consequences of this force. The earliest attempts to quantify magnetic stirring consisted of taking a transverse slice through the problem. That is, the axial variations in **F** were neglected, the sides of the pool were considered to be vertical, and end effects were ignored. In effect, this represents uniform stirring of a long, deep column of radius R. Although this is a natural first step, it turns out that this idealisation is quite misleading, as we shall now show.

These z-independent models are characterised by the fact that **F** drives a one-dimensional swirl flow $u_\theta(r)$. There are no inertial forces and so rings of fluid simply slide over each other like onion rings, driven by F_θ

Downloaded from https://www.cambridge.org/core. NYU School of Medicine, on 13 Nov 2018 at 19:51:53, subject to the Cambridge Core terms of use, available at https://www.cambridge.org/core/terms. https://doi.org/10.1017/CBO9780511760334.011
Cambridge Books Online © Cambridge University Press, 2010

and resisted by shear stresses (Figure 8.3a). The Reynolds-averaged Navier–Stokes equation reduces to a balance between the applied Lorentz force and shear:

$$\tau_{r\theta} = \rho\nu r \frac{d}{dr}\left(\frac{u_\theta}{r}\right) - \rho\overline{v_r v_\theta} = -r^{-2}\int_0^r F_\theta r^2 dr \tag{8.6}$$

Here ν is the viscosity, v represents the fluctuating component of velocity and the overbar denotes a time average. In fact we have already met this problem. We used a simple mixing length model to estimate $\overline{v_r v_\theta}$ in Chapter 5, Section 5.1. Integration of (8.6) is then straightforward. The results are best expressed in terms of a quantity Ω_f defined by

$$\Omega_f^2 = \sigma\Omega B^2/\rho \tag{8.7}$$

When **B** is uniform and $f = 1$, equation (8.6) yields

$$(u_\theta/r)_{r=0} = \Omega_f\{\Omega_f R^2/16\nu\} \tag{8.8}$$

(Laminar flow)

$$(u_\theta/r)_{r=0} = \Omega_f\left\{\frac{1}{2\sqrt{2}\kappa}\ln\left(\frac{\Omega_f R^2}{\nu}\right) + 1.0\right\} \tag{8.9}$$

(Turbulent flow)

These correspond to (5.29) and (5.31). Note that $\kappa = 0.4$ is Karman's constant. When the surface at $r = R$ is rough and dendritic, rather than smooth, the mixing length estimate of $\overline{v_r v_\theta}$ must be modified slightly. The required modification is well known in hydraulics and it turns out that, if k^* is the typical roughness height, then (8.9) becomes

$$(u_\theta/r)_{r=0} = \Omega_f\left\{\frac{1}{2\sqrt{2}\kappa}\ln\left(\frac{R}{k^*}\right)\right\} \tag{8.10}$$

(Turbulent flow, rough wall)

Note that in a turbulent flow u_θ scales linearly with $|\mathbf{B}|$ (with a possible logarithmic correction), whereas in a laminar flow u_θ scales linearly as $\mathbf{B}^2$. These results are summarised in Figure 8.3(b).

Expressions (8.9) and (8.10) were first given by Davidson & Hunt (1987). However, there were many earlier 'numerical experiments'. (Computerised integrations of the Navier–Stokes equation for particular values of B, R, Ω, σ, etc.) For example, Tacke & Schwerdtfeger (1979) integrated the time-averaged Navier–Stokes equations and used a popu-

Downloaded from https://www.cambridge.org/core. NYU School of Medicine, on 13 Nov 2018 at 19:51:53, subject to the Cambridge Core terms of use, available at https://www.cambridge.org/core/terms. https://doi.org/10.1017/CBO9780511623233.011
Cambridge Books Online © Cambridge University Press, 2010

lar, if rather complex, two-parameter turbulence model to estimate the Reynolds stresses. (They used a variant of the popular k–ε model.) However, their results are very similar to the mixing length predictions above.

There were many other numerical experiments, but unfortunately *all* predictions based on integrating (8.6) are substantially out of line with the experimental data, no matter what turbulence model is used![2] The key point is that the force balance (8.6) relies on the time-averaged inertial forces being exactly zero. However, in practice, there are always significant secondary flows $(u_r, 0, u_z)$ induced, for example, by Ekman pumping on the base of the pool (see Chapter 3, Section 7 for a discussion of Ekman pumping). This secondary motion ensures that the inertial forces are finite. Indeed, when Re is large, as it always is, we would expect the inertial forces to greatly exceed the shear stresses, except near the boundaries. Consequently, in the core of the flow, the local force balance should be between F_θ and inertia, not between F_θ and shear. To obtain realistic predictions of $\mathbf{u}$ we must embrace the three-dimensional nature of the problem, seek out the sources of secondary motion, and incorporate these into the analysis.

Some hint as to the rôle of secondary motion appears in the example discussed in Chapter 5, Section 5.2. Here we looked at the laminar flow of a liquid held between two flat, parallel plates and subject to the force (8.3). It was found that Ekman-like layers form on the top and bottom surfaces, and that these layers induce a secondary, poloidal flow as shown

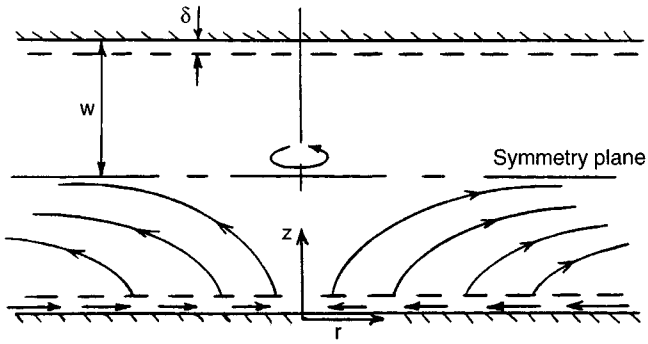

Figure 8.4 Swirling flow between two discs driven by the force $F_\theta = \frac{1}{2}\sigma\Omega B^2 r$.

[2] See Davidson & Hunt, 1987, and Davidson, 1992.

Downloaded from https://www.cambridge.org/core. NYU School of Medicine, on 13 Nov 2018 at 19:51:53, subject to the Cambridge Core terms of use, available at https://www.cambridge.org/core/terms. https://doi.org/10.1017/CBO9780511626333.011
Cambridge Books Online © Cambridge University Press, 2010

in Figure 8.4. We showed that, outside the Ekman (or Bodewadt) layers, the viscous stresses are negligible and the fluid rotates as a rigid body, the rotation rate being quite different to that predicted by (8.8). In fact, the core rotation is

$$\Omega_c = 0.516\Omega_f\left[\Omega_f w^2/\nu\right]^{1/3} \tag{8.11}$$

where $2w$ is the distance between the plates. Moreover, we saw that the Ekman layers are unaffected by the presence of the forcing (the Lorentz force is negligible by comparison with the viscous forces) and so they look like conventional Bodewadt layers. For example, the thickness of the boundary layer is of the order of $\delta \sim 4(\nu/\Omega)^{1/2}$.

This simple model problem is discussed at some length in Davidson (1992), where the key features are shown to be:

(i) the flow may be divided into a forced, inviscid core, and two viscous boundary layers in which the Lorentz force is negligible;
(ii) all of the streamlines pass through both regions, collecting energy in one region and losing it in the other;
(iii) the applied Lorentz force in the core is exactly balanced by the Coriolis force.

We shall see shortly that all of these features are characteristic of stirring an aluminium ingot. The main point, however, is (iii). When a secondary flow is present, the Lorentz force is balanced locally by inertia, not shear, and this is why (8.8) and (8.11) look so different. An important question is, therefore: what kinds of secondary flow occur during the stirring of an ingot?

From an industrial perspective there are two distinct cases of particular interest. The first is where the pool is as deep as it is broad, which is typical of aluminium casting. Here the source of secondary motion is Ekman pumping, as in the model problem above. The second case is where we have a long column of liquid, but with the stirring force F_θ applied over a short portion of that column. This is relevant to the casting of steel, and in this case the secondary motion arises from differential rotation along the length of the column. We shall consider each of these in turn, starting with pools which are roughly hemi-spherical or parabolic in shape.

Downloaded from https://www.cambridge.org/core. NYU School of Medicine, on 13 Nov 2018 at 19:51:53, subject to the Cambridge Core terms of use, available at https://www.cambridge.org/core/terms. https://doi.org/10.1017/CBO9780511613333.011
Cambridge Books Online © Cambridge University Press, 2010

8.3 The Dominance of Ekman Pumping in the Stirring of Confined Liquids

Suppose that the pool has an aspect ratio of the order of unity, as indicated in Figure 8.2(a). We make no particular assumptions about the shape of the boundary, although we have in mind profiles which are roughly parabolic. It turns out that this is a long-standing and much studied problem, and not just in the case of aluminium casting. For example, Zibold et al. (1986) looked at magnetically forced swirl in a cylindrical cavity in the context of single crystal pulling. Bojarevics & Millere (1982) studied the equivalent problem in a hemisphere, motivated by problems in electric-arc welding, while Vlasyuk & Sharamkin (1987) and Muizhnieks & Yakovich (1988) looked at forced swirl in paraboloids and cylinders, motivated this time by vacuum-arc remelting of ingots. All of these studies were, in effect, numerical experiments. (Integrations of Navier–Stokes equation for particular values of B, Ω, R, σ, ν, etc.) However, as we shall see, it is possible to develop a single unified model which encapsulates all of these studies.

The key to establishing the distribution of swirl lies in the simple, text-book problem of 'spin-down' of a stirred cup of tea (Figure 8.5). (This is discussed in Chapter 3, Section 7.) In this well-known example, the main body of the fluid is predominantly in a state of inviscid rotation. The associated centrifugal force is balanced by a radial pressure gradient, and this pressure gradient is also imposed throughout the boundary layer on the base of the cup. Of course, the swirl in this boundary layer (the Ekman layer) is diminished through viscous drag, and so there is a local imbalance between the radial pressure force and u_θ^2/r. The result is a radial inflow along the bottom of the cup, with the fluid eventually drifting up and out of the boundary layer. In short, we

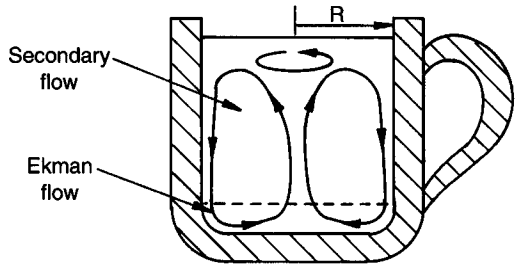

Figure 8.5 Spin-down of a stirred cup of tea.

Downloaded from https://www.cambridge.org/core. NYU School of Medicine, on 13 Nov 2018 at 19:51:53, subject to the Cambridge Core terms of use, available at https://www.cambridge.org/core/terms. https://doi.org/10.1017/CBO9780511623332.011
Cambridge Books Online © Cambridge University Press, 2010

have a kind of Bodewadt layer. Of course, continuity then requires that the boundary layer is replenished via the side walls and the end result is a form of Ekman pumping, as shown above. As each fluid particle passes through the Ekman boundary layer, it gives up a significant fraction of its kinetic energy and the tea finally comes to rest when all the contents of the cup have been flushed through the Ekman layer. The spin-down time, therefore, is of the order of the turn-over time of the secondary flow.

It is useful to consider a variant of this problem. Suppose now that the tea is continuously stirred. Then it will reach an equilibrium rotation rate in which the work done by the tea-spoon exactly balances the dissipation in the Ekman layers. This provides the clue to analysing magnetic stirring, and we now return to this problem.

Suppose we integrate the time-averaged Navier–Stokes equations around a streamline which is closed in the r–z plane. For a steady flow, we obtain

$$\oint \mathbf{F} \cdot d\mathbf{x} + \nu_t \oint \nabla^2 \mathbf{u} \cdot d\mathbf{x} = 0 \tag{8.12}$$

Here ν_t is an eddy viscosity which for simplicity we treat as constant, and $\mathbf{F}$ is the Lorentz force per unit mass. This is an energy balance: it states that all of the energy imparted to a fluid particle by the Lorentz force must be destroyed or diffused away by shear before it returns to its original position. However, the shear stresses are significant only in the boundary layers. By implication, *all* streamlines must pass through a boundary layer. Of course, Ekman pumping provides the necessary entrainment mechanism. Note also that Ekman layers can and will

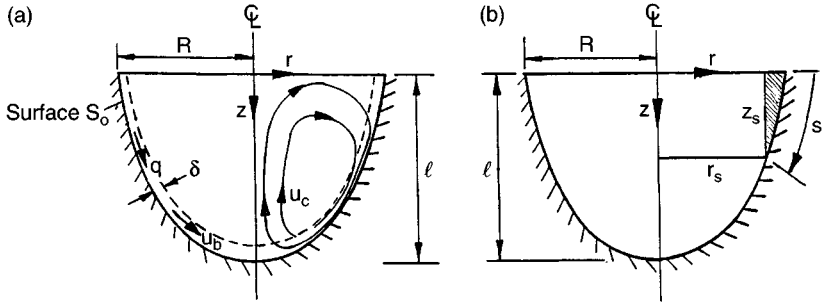

Figure 8.6 (a) Secondary (poloidal) flow induced by swirl in a cavity. (b) Coordinate system.

Downloaded from https://www.cambridge.org/core. NYU School of Medicine, on 13 Nov 2018 at 19:51:53, subject to the Cambridge Core terms of use, available at https://www.cambridge.org/core/terms. https://doi.org/10.1017/CBO9780511800313.033
Cambridge Books Online © Cambridge University Press, 2010

form on all surfaces non-parallel to the axis of rotation. The structure of the flow, therefore, is as shown in Figure 8.6(a) (Davidson, 1992). It consists of an interior body of (nearly) inviscid swirl surrounded by Ekman wall jets on the inclined surfaces. Each fluid particle is continually swept first through the core, where it collects energy and angular momentum, and then through the Ekman layers, where it deposits its energy. The motion is helical, spiralling upwards through the core, and downwards through the boundary layers.

The fact that all streamlines pass through the Ekman layers has profound implications for the axial distribution of swirl. Let u_b and u_c be characteristic values of the poloidal recirculation $(u_r, 0, u_z)$ in the boundary layer and in the core. Also, let δ be the boundary layer thickness, R be a characteristic linear dimension of the pool, and $\Gamma = u_\theta r$ be the angular momentum. Now u_b and u_θ are of similar magnitudes (one drives the other) and so continuity requires that

$$u_c \sim u_b(\delta/\mathrm{R}) \sim \mathrm{u}_\theta(\delta/\mathrm{R}) \tag{8.13}$$

That is, the core recirculation is weak. However, the core recirculation is related to the core angular momentum, Γ_c, by the inviscid vorticity equation

$$\mathbf{u} \cdot \nabla(\omega_\theta/r) = \frac{\partial}{\partial z}\left(\frac{\Gamma_c^2}{r^4}\right) \tag{8.14}$$

Combining (8.13) and (8.14) we have (Davidson, 1992)

$$\Gamma_c = \Gamma_c(r)\left[1 + O(\delta/R)^2\right] \tag{8.15}$$

It is extraordinary that, no matter what the spatial distribution of the Lorentz force, the induced swirl is independent of height to second order in (δ/R). This prediction has been confirmed in the experiments of Davidson, Short & Kinnear (1995), where highly localised distributions of F_θ were used.

Since the flow has a simple, clear structure, it is possible to piece together an approximate, quantitative model of the process. We give only a schematic outline here, but more details may be found in Davidson (1992). In the inviscid core the applied Lorentz force is balanced by inertia: $(\mathbf{u} \cdot \nabla)\Gamma_c = rF_\theta$. Since Γ_c is a function only of r, the left-hand side reduces to $u_r\Gamma_c'(r)$, the Coriolis force. Thus,

$$u_r = rF_\theta/\Gamma_c'(\mathrm{r}) \tag{8.16}$$

Downloaded from https://www.cambridge.org/core. NYU School of Medicine, on 13 Nov 2018 at 19:51:53, subject to the Cambridge Core terms of use, available at https://www.cambridge.org/core/terms. https://doi.org/10.1017/CBO9780511623233.011
Cambridge Books Online © Cambridge University Press, 2010

Now all the fluid which moves radially outward is recycled via the boundary layer and so (8.16) may be used to calculate the mass flux in the Ekman layer. In particular, if we apply the continuity equation to the shaded area in Figure 8.6(b) we obtain an estimate of the mass flux in the boundary layer:

$$\dot{q} = 2\pi r_s \int_0^{\delta} u_b dn = 2\pi r_s \int_0^{z_s} u_r dz = \frac{1}{\Gamma_c'(r_s)} \frac{dT}{dr_s} \tag{8.17a}$$

where

$$T = \int_0^{r_s} \int_0^{z_s} 2\pi r^2 F_\theta dr dz \tag{8.17b}$$

Here T is the total magnetic torque applied to the fluid between $r = 0$ and $r = r_s$, where (r_s, z_s) represents the coordinates of the boundary (Figure 8.6(b)). Also, n is a coordinate measured from the boundary into the fluid, and $u_b(n)$ is the velocity profile in the boundary layer.

Next, we turn our attention to the boundary layer. Equation (8.16) tells us that the ratio of the Lorentz force to inertia in the boundary layer is $rF_\theta/(\mathbf{u} \cdot \nabla\Gamma) \sim (u_c\Gamma_c/R)/(u_b\Gamma_c/R) \sim \delta/R$. Since ($\delta \ll R$ we may neglect F_θ in the boundary layer and the azimuthal equation of motion reduces to

$$(\mathbf{u} \cdot \nabla)\Gamma = \text{viscous terms}$$

In integral form this becomes

$$\oint_S \Gamma \mathbf{u} \cdot d\mathbf{S} \sim \oint_S (\text{viscous stresses}) d\mathbf{S}$$

where S is any closed surface. This states that the net flux of angular momentum out of some closed surface is proportional to the viscous torque acting on that surface. Frequently, in boundary layer analysis, it is useful to apply an integral equation of this form to a short portion of the boundary layer. (This is equivalent to integrating the equation of motion across the boundary layer.) The result is referred to as a momentum integral equation, and in this case the azimuthal integral equation takes the form (see Davidson, 1992)

$$\frac{\dot{q}}{\pi} \frac{d\Gamma_c}{ds} - \frac{d}{ds}\left\{ \chi \Gamma_c \left[\frac{\dot{q}}{\pi} \right] \right\} = -c_f \Gamma_c^2 \tag{8.18}$$

Here c_f is the dimensionless skin-friction coefficient, $\tau_\theta/(\frac{1}{2}\rho u_\theta^2)$, χ is a shape factor related to the velocity profile in the Ekman wall jet (usually

Downloaded from https://www.cambridge.org/core. NYU School of Medicine, on 13 Nov 2018 at 19:51:53, subject to the Cambridge Core terms of use, available at https://www.cambridge.org/core/terms. https://doi.org/10.1017/CBO9780511626333.011
Cambridge Books Online © Cambridge University Press, 2010

taken as 1/6), and s is a curvilinear coordinate measured along the boundary from the surface. (Typically, $c_f = 0.052(\Gamma_c/\nu)^{-1/5}$). Eliminating $\dot{q}$ from (8.17a) and (8.18) furnishes

$$\frac{dT}{ds} - \frac{d}{ds}\left\{\chi \frac{\Gamma_c}{\Gamma_c'(s)} \frac{dT}{ds}\right\} = -\pi c_f \Gamma_c^2 \tag{8.19}$$

This simple o.d.e. allows the distribution of the core swirl, $\Gamma_c(r)$, to be calculated whenever the applied Lorentz torque, T, is known. It applies to any shape of cavity and any distribution of F_θ, and so provides a unified model of forced swirl in a cavity. For example, in hemispheres with $f = 1$ it predicts a maximum value of Γ_c of $0.42\Omega_f R^2 c_f^{-1/2}$, so that Γ scales as $F_\theta^{5/9}$. The predictions of (8.19) have been tested against experiments performed in cones, hemispheres and cylinders, and there is a reasonable correspondence between theory and experiment. (Davidson et al. 1995.) However, perhaps the most important results are (i) the existence of the Ekman wall jets, which sweep down the solidification front carrying crystal fragments with them, and (ii) equation (8.15), which shows that the fluid is quite insensitive to the detailed distribution of the applied Lorentz force. It cares only about the globally averaged torque. This model has been generalised to unsteady flows by Ungarish (1997).

8.4 The Stirring of Steel

The simplest idealisation of the magnetic stirring of steel is that shown in Figure 8.2(b). That is, the fluid occupies a long cylindrical column, while the Lorentz force, F_θ, is applied over a relatively short portion of that column. Evidently, there is no Ekman pumping and we must seek a different way of satisfying (8.12). Once again, the secondary flows turn out to be crucial. This time the secondary (poloidal) motion is generated by differential rotation between the forced and unforced regions of the column. The relatively low pressure on the axis of the more rapidly rotating fluid causes the magnetic stirrer to act like a centrifugal pump (Figure 8.7). Fluid is drawn in from the far field, moving along the axis towards the magnetic field. It enters the forced region, is spun up by the Lorentz force and is then thrown to the walls. Finally, the fluid spirals down the solidification front where, eventually, it loses its excess energy and angular momentum through wall shear. In the steady state the fluid cannot return until its excess energy is lost (c.f. (8.12)), and it takes a long time for the boundary layers on the outer cylindrical walls to

Downloaded from https://www.cambridge.org/core. NYU School of Medicine, on 13 Nov 2018 at 19:51:53, subject to the Cambridge Core terms of use, available at https://www.cambridge.org/core/terms. https://doi.org/10.1017/CBO9780511623233.011
Cambridge Books Online © Cambridge University Press, 2010

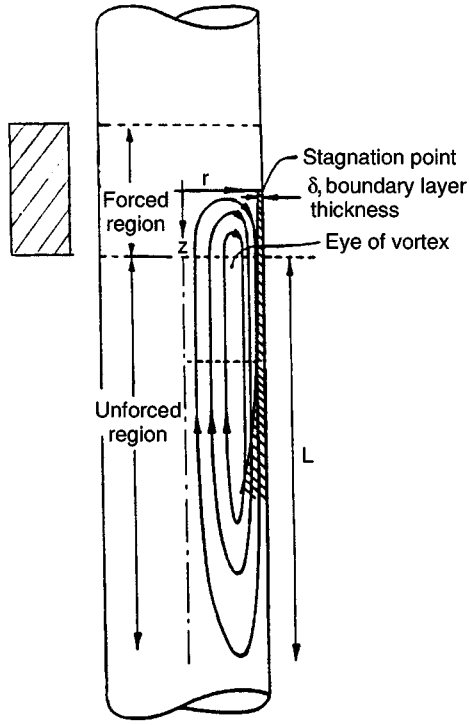

Figure 8.7 Secondary flow in the stirring of steel.

dissipate this energy, essentially because the cross-stream diffusion of energy to the wall is a slow process. Consequently, this centrifugal pumping ensures that a very long portion of the liquid metal column is eventually set into rotation (of order $l \sim u_\theta R^2/\nu_t$), even though F_θ is restricted to a relatively short part of the column. The picture, therefore, is one of fluid being continuously cycled first through the forced region, where it is spun up, then through the side-wall boundary layers, where energy is lost. Note that the local force balance is between inertia ($\mathbf{u} \cdot \nabla \Gamma$) and the applied torque, rather than between F_θ and shear. As a consequence, one-dimensional models of the form discussed in Section 8.2 over-estimate the induced swirl by a factor of around five! (Davidson & Hunt, 1987.) An approximate analytical model of this flow has been proposed by Davidson Hunt, which predicts that the maximum swirl occurs, not where F_θ is largest, but rather at the upper and lower edges of the forced region, where F_θ falls to zero. This has

Downloaded from https://www.cambridge.org/core. NYU School of Medicine, on 13 Nov 2018 at 19:51:53, subject to the Cambridge Core terms of use, available at https://www.cambridge.org/core/terms. https://doi.org/10.1017/CBO9780511613333.011
Cambridge Books Online © Cambridge University Press, 2010

been confirmed by experiment. Yet again, we see that the spatial distribution of swirl does not mimic that of F_θ, and that secondary (poloidal) flows play a key rôle in the overall dynamics.

From a practical point of view perhaps the most important point to note is that the swirl generated by a stirrer will penetrate many diameters above and below the stirrer. This gives the designer some latitude in his choice of location of the device.

Examples

8.1 Estimate the magnitude of swirl, u_θ, in terms of the force, F_θ, induced by the localised stirring of a long steel strand. (Hint: first estimate the relationship between $\mathbf{u}_p$ and u_θ.)

8.2 Show that the depth of stirring induced in a long steel column by a localised Lorentz force is of order $l \sim u_\theta R^2/\nu_t$. Use two different methods: (1) perform an overall torque balance on the column; and (2) estimate the rate of growth of the boundary layer on the wall $r = R$.

8.3 Derive the momentum equation (8.18) by integrating the azimuthal equation of motion across the boundary layer.

8.4 By considering the appropriate overall torque balance, explain why one-dimensional models of stirring will always overestimate the localised stirring in a long steel strand by an order of magnitude.

Downloaded from https://www.cambridge.org/core. NYU School of Medicine, on 13 Nov 2018 at 19:51:53, subject to the Cambridge Core terms of use, available at https://www.cambridge.org/core/terms. https://doi.org/10.1017/CBO9780511333611.011
Cambridge Books Online © Cambridge University Press, 2010